Received: 13 December 2024 | Revised: 13 April 2025 | Accepted: 19 May 2025

DOI: 10.1002/cjce.70004

RESEARCH ARTICLE

THE CANADIAN JOURNAL OF CHEMICAL ENGINEERING

Thermal degradation of impact-modified PMMA in mechanical and chemical recycling

Tien Dat Nguyen[1] | **Nooshin Saadatkhah**[1] | **Yanfa Zhuang**[1] | **Jacopo De Tommaso**[1] | **Karen Stoeffler**[2] | **Adrien Faye**[2] | **Gregory S. Patience**[1]

[1]Chemical Engineering, Polytechnique Montréal, Montréal, Québec, Canada

[2]Automotive and Surface Transportation Research Center, National Research Council of Canada, Boucherville, Québec, Canada

Correspondence
Gregory S. Patience, Chemical Engineering, Polytechnique, Montréal, C.P. 6079, Succ. "CV", Montréal, H3C3A7 QC, Canada.
Email: gregory-s.patience@polymtl.ca

Funding information
National Research Council of Canada (NRC) Collaborative Science, Technology and Innovation Program (CSTIP), Grant/Award Number: AM-102-1; Recycling Technologies for polymer Automotive Components

Abstract

Poly (methyl methacrylate) (PMMA) is a thermoplastic with outstanding tensile strength, UV resistance, and a high level of transparency that has been used widely for optical applications such as glazing in the automobile industry. Mechanical recycling, the most widespread method, degrades the physical properties and prevents reusing PMMA in transparent applications. Thermal depolymerization to recover methyl methacrylate (MMA) monomer is becoming an alternative route for PMMA recycling. In this paper, the thermal depolymerization process of impact-modified PMMA in a micro fluidized bed reactor was investigated. The pyrolysis was conducted over aluminium oxide (Al_2O_3) and fluid-cracking catalyst (FCC) as catalytic beds; sand and SiC as inert beds at temperatures below 400°C. A mechanical recycling process was also simulated using sequential injection moulding to investigate its impact on the properties of PMMA. After 5 cycles of injection moulding, the impact strength and optical properties of PMMA were severely diminished due to an increase in free volume and partial thermal degradation. Regarding PMMA pyrolysis, Al_2O_3 demonstrated limited cracking ability with a maximum MMA yield of 46%, as opposed to FCC, which over-cracked both PMMA and MMA into coke and unwanted products. In contrast, non-catalytic beds exhibited higher activity for MMA recovery, with SiC yielding the highest amount of 92% at 380°C.

KEYWORDS

fluidized bed, polymethyl methacrylate, sequential injection moulding, thermal degradation

1 | INTRODUCTION

PMMA is a transparent thermoplastic with outstanding impact strength, UV resistance, and transmittance, with a total global market value of 5.2 billion US dollars in 2022 and an annual growth rate forecasted at 3.5% from 2023 to 2030.[1] COVID-19 shut down multiple manufacturing facilities and the supply chain severely plummeted the consumption rate of most plastic types except PMMA. The demand for transparent sheets for protective barriers rocketed in 2020, which even elevated the price of this polymerf by 25%.[2] The market growth for this plastic

follows the anticipated trend as the effort to make lighter vehicles is becoming more attractive in the automotive industry. As a consequence, PMMA waste surpasses the present ability of recycling, as only 8 kt out of 300 kt PMMA/year are recycled, with up to 70% coming from unqualified products or remnant waste from mechanical processing steps.[3]

One of the most common methods to mitigate the plastic waste crisis is mechanical recycling, where PMMA is blended with virgin material to lengthen its life cycle. To meet the requirements of the automotive industry, recycled plastic must retain both mechanical and optical properties. Extrusion and injection moulding are the most common techniques to reprocess plastic at the industrial scale. Efforts on reprocessing PMMA with an extruder have been studied to exploit its optical properties.[4] Minor degradation was observed, as a consequence of the random scission in the carbon chain when the temperature was higher than 230°C and under mechanical stress inside the extruder barrel.[5] This issue restricts the reusability of plastic to a limited number of cycles, as the more it is reprocessed, the higher the amount of impurities accumulate that compromise the optical and mechanical properties.[6]

Chemical recycling is optimal for PMMA; at temperatures between 350 and 450°C, it degrades to pure MMA with a yield higher than 90%.[7–9] Virgin plastics decompose to pure monomers, while end-of-life waste, which contributes the major amount of total PMMA waste, contains plasticizers to improve the polymer's thermal and mechanical stability. For automotive applications, elastomeric polymers (MBS, ABS, linear co-polymers of butadiene with styrene, etc.) are blended with PMMA to form 'impact-modified' plastic which affects the purity and yield of monomers in thermal decomposition step.[10–12] Additives are prone to coking which leads to catalyst deactivation by active site coverage and by pore blockage, restricting the diffusion of the reactants.[13,14] Crosslinking and fillers in the polymer matrix also shift the thermal decomposition pathway to produce by-products instead of pure MMA.[7] Available technologies to pyrolyze PMMA operate at 400°C.[15] This high temperature engenders high capital investment and operational costs. Cracking catalysts zeolites ZSM-5, BETA, and USY lower the PMMA degradation temperature and improve monomer recovery.[16,17] Because the polymerization mechanism follows a radical pathway,[18] the agent contains highly reactive hydroxyl radicals as H_2O_2 accelerates the decomposition.[19]

Monomer yields from PMMA pyrolysis also depend on heat and mass transfer which depends on various reactor configurations.[8] Among technologies to chemically recycle PMMA, fluidized bed reactors have the highest heat and mass transfer rates without contamination from organometallic compounds in the product stream and less coke in the solid residue.[7,20] However, the solid bed easily defluidizes at temperatures below 400°C.[21] This phenomenon commonly occurs due to the agglomeration of the bed when plastic becomes softened and sticky.[22] Besides temperature, the plastic–catalyst mass ratio is a critical parameter for maintaining stable fluidization.[21–23]

Here we investigate the effect of a sequential injection moulding process that simulates mechanical recycling cycle on physical and optical properties of impact-modified PMMA. The recyclability of this polymer is evaluated through catalytic pyrolysis over Al_2O_3 and FCC fluidized bed in a micro reactor to lower the degradation temperature of PMMA as well as maximize the yield of monomer produced. Sand and SiC with good chemical stability at temperatures up to 1000°C are used to compare with the catalytic beds.[24,25]

2 | EXPERIMENTAL

2.1 | Materials

Impact-modified PMMA grade (ALTUGLAS® HFI-15) was provided by NRC. Coarse powder for thermal depolymerization tests was obtained by cryogenic milling in liquid N_2. Activated acidic gamma Al_2O_3 was purchased from Sigma-Aldrich and faujasite-type fluid catalytic cracking catalyst (FCC) from a commercial brand (W.R. Grace). Commercial sand was washed with deionized water and dried at 80°C for 1 day. Silicon carbide black (98%) was purchased from Sigma-Aldrich Supelco. All the solids were sieved to achieve a particle size range from 63 to 106 μm. Gas bottles were provided by Air Liquide Canada: argon (>99.7%), a mixture of CO (1.05%), CO_2 (0.984%), CH_4 (1.02%) with balance argon and a mixture of CO (14.5%), CO_2 (14.6%), CH_4 (16%), H_2 (20.3%) with balance argon.

2.2 | Characterization

2.2.1 | Optical properties test

After the mechanical recycling test, a BYK Gardner hazegard plus instrument measures 3 transmittance, haze and clarity at three positions of a dogbone produced from injection moulding. The samples are conditioned at 23°C and 50% relative humidity (RH) for 48 h. Each test was repeated 3 times ($n = 3$).

2.2.2 | Mechanical properties test

The tensile strength tests were performed with an Instron Universal Testing System based on the ASTM D638

standard.[26] The crosshead speed was set at 50 mm/min for the tensile strength tests, while measuring the tensile modulus (Young's modulus) required an external extensometer to measure small changes in sample strain and the crosshead speed was reduced to 1 mm/min.

Impact strength tests were performed by a Charpy Impact Tester based on the ASTM D256 standard.[27] The specimens were notched with a radius of 1.75 mm. Virgin samples (represent cycle 0) for the impact strength test were produced by compression moulding: the virgin plastic pellets were filled into moulds that satisfy the ASTM D256 standard. After that, the moulds were heated to 200°C before being compressed to 30 kN. The samples were cooled for 2 h to ambient temperature. After removing from the moulds, they were inspected for imperfections and internal bubbles, then we trimmed the edges to create smooth surfaces.

All samples were pre-conditioned in a vacuum oven at 80°C for 24 h, then 48 h at room temperature, 50% RH. Every test was repeated 5 times ($n = 5$).

2.2.3 | Free volume determination

Free volume—the space for polymer chain to move around—is determined by the following:

$$v_f = v - v_* = v - K \times M_w \quad (1)$$

where v_f is free volume; v is specific volume; v_* is occupation volume, which is assumed to correlate linearly with the average weight molecular weight M_w; and K is a coefficient equal to 7.8×10^{-6} mL moleg^{-2}.[6,28]

2.2.4 | X-ray powder diffraction (XRD)

The X-ray diffraction patterns of FCC and Al_2O_3 were produced with a Bruker D8 advance diffractometer with Cu Kα radiation in the 2θ angle of 5° to 90° (scanning step = 0.02°).

2.2.5 | Thermogravimetric analysis (TGA)

A TA Instrument Q500 Thermogravimetric Analyzer recorded the PMMA pellet degradation pattern at 60 mL/min of N_2.[15,29] The sample first was ramped up from room temperature to 600°C with a heating rate of 10°C/min and kept isothermal at this temperature for 20 min. The sample then was heated up to 800°C with the same ramp in air to combust the remaining organic compounds.

The solid residues after reactions were also analyzed by TGA method. The temperature programmed progressed similarly to the test with pure plastic: a 10°C/min ramp to 600°C in N_2, a 20-min isothermal step and lastly a ramp to 800°C in air. To ensure isothermal conditions, for each test we use approximately 15 mg of sample.

2.2.6 | Differential scanning calorimetry (DSC)

A TA Instrument Q2000 DSC analyzer measured the glass transition temperature (T_g) of PMMA. At the beginning of the test, the aluminium capsule containing the sample was heated to 180°C to remove its thermomechanical history. Quenching to 40°C followed afterward, before the calorimeter ramped up to 180°C at rate of 10°C/min. Meanwhile, a N_2 flow of 50 mL/min purged the system to maintain an inert atmosphere.

2.2.7 | N_2 adsorption

A Quantachrome Autosorb-1 physisorption analyzer measured the total specific surface area and pore volume of catalysts by N_2 adsorption at 77 K. The samples were vacuum-degassed at 250°C for 24 h in advance. The construction of Brunauer–Emmett–Teller (BET) plot of P/P_0 range between 0.05 and 0.35 gives the total specific surface area. The total pore volume was determined at the transition point of adsorption–desorption processes where $P/P_0 = 0.99$. From isothermal curve data at 77 K, the pore size distribution and average pore size were calculated based on the Barrett–Joyner–Halenda (BJH) model.

2.2.8 | Particle size distribution (PSD)

A laser diffractometer Horiba LA950 determines the particle size distribution of solid catalysts. Each test was repeated twice.[30]

2.2.9 | Gel permeation chromatography (GPC)

A Thermo Scientific UltiMate 3000 HPLC system coupled Refractive Index (RI) detector quantified the average molecular weight of PMMA (M_w). Two tandem columns Shodex GPC KF-803 L and KF-804 L separated the polymer chains based on their size in THF. The flow rate was set at 1 mL/min and temperature of detector at 35°C; each test lasted 60 min. Prior to injecting samples to GPC system, we dissolved virgin PMMA and PMMA standards from Shodex STANDARD M-75 kit in THF for 1 day.

2.2.10 | Gas, liquid, and solid products composition quantification

A Hiden HPR-20 QIC TMS mass spectrometer (MS) equipped with a quartz inert capillary monitored the gaseous effluent from the reactor, including CO, CO_2, and CH_4. Specific mass fragments were assigned for each gas: CO—28 amu; CO_2—44 amu; and CH_4—15 amu. Prior to the experiment, we calibrated the MS using a mixture of CO (1.05%), CO_2 (0.984%), CH_4 (1.02%), and a mixture of CO (14.5%), CO_2 (14.6%), and CH_4 (16%) (Air Liquide) to obtain the correlation between recorded signal and concentration of gas. The MS recorded signal reflecting the progress of reaction continuously until the concentration of gas approached zero. The total mole of gas i produced n_i was calculated by the product of concentration (N_i) over time and the total flow rate of non- condensable gases (Q).

$$n_i = \frac{Q \times \int_0^t N_i \mathrm{d}t}{22.4} \tag{2}$$

where t is reaction time and 22.4 is the molar volume of one gas mole at standard condition.

An Agilent 7890A GC equipped with an autosampler and 5975C mass selective detector (MSD) mass spectrometer determined the liquid products' composition and concentration. An ultra inert (UI) capillary column, Agilent J&W DB-Wax UI (polyethylene glycol stationary phases, length 30 m, inner diameter 0.25 mm, film thickness 0.25 μm), separated products in the collected mixtures. Full scan test with m/z from 29 to 500 revealed the structure of each compound in the mixture. Selected ion monitoring (SIM) mode was used to quantitatively analyze acetone (selected m/z 43 and 58) and MMA (selected m/z 69 and 100). External calibration standards contained MMA (≥99.6%, stabilized with 6-tert-Butyl-2, 4-xylenol, Sigma-Aldrich) and acetone (HPLC grade, ≥99.9% Sigma-Aldrich) diluted with anhydrous ethanol (HPLC grade, commercial alcohols).

The catalytic activity is determined from conversion (X), selectivity (S) and yield (Y) from the GC–MS:

$$\begin{aligned} X_{\mathrm{PMMA}} &= \frac{\text{PMMA weight inlet} - \text{PMMA weight residue}}{\text{PMMA weight inlet}} \times 100 \\ S_i &= \frac{\text{moles of product } i \text{ collected} \times C_i}{\text{moles of MMA collected} \times 5} \times 100 \\ Y_i &= \frac{\text{moles of product } i \text{ collected} \times C_i}{\text{correspond MMA moles inlet} \times 5} \times 100 \end{aligned} \tag{3}$$

when i is the compound produced and C_i is the number of carbon atoms per compound i.

The preliminary TGA result for Al_2O_3 bed (Figure A2) indicated that the amount of coke in the residue is negligible. Therefore, the total weight of PMMA residue (g) is calculated from the TGA curve by the following:

$$\begin{aligned} m_{\text{total PMMA residue}} = {} & m_{\text{lost PMMA residue}} \\ & + m_{\text{lost PMM Acoking}} + m_{\text{lost total coke}} \end{aligned} \tag{4}$$

In the case of FCC, preliminary thermogravimetric analysis (TGA) indicated a substantial amount of coke present in the solid residue (Figure A3). We assumed that the coke generated during the TGA process is considerably less than the amount initially present in the sample. Therefore, the total weight of PMMA residue (g) is calculated by the following:

$$\begin{aligned} m_{\text{total PMMA residue}} = {} & m_{\text{lost PMMA residue}} \\ & + m_{\text{lost PMMA coking}} \end{aligned} \tag{5}$$

For the solid residue, a LECO CS744 analyzer coupled with an IR detector determined the total mass fraction of carbon inside solid residue by combustion at 1300–1400°C accelerated by iron and tungsten.

2.3 | Sequential mechanical recycling equipment and experiment procedure

The polymer was dried in a Conair drier for 4 h at 80°C, before being injection-moulded using a Boy 30A injection-moulding machine. Standard specimens for tensile testing (ASTM D638–type 1) and impact testing (ASTM D256–type 1) were produced. Temperatures at barrels varied from 230 to 245°C, while the mould was kept at 80°C. Thirty samples of each cycle were retained for further characterization. The rest were ground in a Brabender grinder and reused for the next cycle of injection moulding. This sequence was repeated four times.

2.4 | PMMA pyrolysis in fluidized bed

2.4.1 | Design of experiment (DOE)

To screen the effect of catalysts and reaction conditions on monomer yield in PMMA pyrolysis, we applied a Plackett–Burman partial factorial design with four factors (Table 1). The mass ratio plastic/catalysts increase proportionally with the defluidization time.[22] To minimize defluidization, this ratio is approximately 10% at pilot scale reactor.[31] Therefore, we use 1 g of PMMA in each

TABLE 1 Design of experiment for fluid-cracking catalyst (FCC) and Al_2O_3.

Run	Catalyst	T (°C)	U_g (mm s^{-1})	m (g)
1	γ-Al_2O_3	380	38	10
2	FCC	380	50	10
3	FCC	350	38	7
4	FCC	350	50	7
5	γ-Al_2O_3	380	50	7
6	γ-Al_2O_3	350	50	10
7	FCC	380	38	7
8	γ-Al_2O_3	350	38	10
9	FCC	380	50	10
10	γ-Al_2O_3	350	38	7
11	FCC	350	50	7
12	γ-Al_2O_3	350	50	10

test and select 2 levels of catalyst mass to study the effect of plastic/catalyst mass ratio on fluidization behavioir in a micro-scale system.

- Temperature, T (2 levels): 350, 380°C;
- Fluidization velocity, U_g (2 levels): 5, 6.7 mm s^{-1};
- Catalyst mass, m (2 levels): 7, 10 g;
- Catalyst type (2 levels): Al_2O_3 and FCC

Sand and SiC were used as non-catalytic media to compare with FCC and Al_2O_3 in terms of monomer yield (Table 2). The minimum fluidization velocities of different beds—U_{mf} were determined by pressure drop method (Figure A8).[32,33]

We injected MMA at 380°C with a fluidization velocity of 38 mm s^{-1} over 10 g of Al_2O_3 and FCC bed separately to evaluate the stability of MMA as well as the cracking ability of both catalysts.

2.4.2 | Reaction equipment and experimental conditions

The micro-fluidized bed reactor consists of a 13 mm ID quartz tube, 740 mm long situated inside a Carbolite vertically mounted furnace. A gas distributor made of glass wool 20 mm thick located in the middle of the reactor to support the powder. The reactor was charged with 1 g of powder PMMA and catalysts (Table 1). A thermocouple attached to the top fittings of the reactor dipped into the powder mixture and measured the average temperature inside the bed. At the bottom of the reactor, a flow of argon controlled by a mass flow controller (MFC) fluidized the system at designated flow rates. The exit line of the reactor was linked with a glass condenser and a 100 mL round bottom flask

TABLE 2 Experimental condition for heat transfer media.

Run	Catalyst	T (°C)	U_g/U_{mf}	m (g)
1	Sand	380	3	7
2	Sand	380	10	7
3	Sand	400	10	7
4	SiC	380	3	7
5	SiC	380	10	7
6	SiC	400	10	7

Abbreviation: SiC, silicon carbide.

containing 80 mL of anhydrous ethanol to absorb the MMA vapour. An additional cold trap trapped any remaining non-condensed compounds. Both apparatuses were cooled by ice-salt mixture. An online MS quantified the concentration of non-condensable gas CO, CO_2, and CH_4. Each test lasted for 35 min.

For the MMA pyrolysis test, a 150 mL stainless steel double-ended Swagelok sample cylinder covered with heating tape and glass wool evaporated liquid from an HPLC Azura P4.1S pump. A second thermocouple was used to monitor the evaporation temperature at 200°C. After the bed reached the target temperature, the pump started dosing MMA into the evaporator at 1 mL/min for 4 min. The amount of MMA input was then verified again by the gravimetric method (Figure 1).

3 | RESULT AND DISCUSSION

3.1 | Average molecular weight

From the GPC result, both average weight molecular weight (M_w) and average number molecular weight (M_n) slightly reduced (less than 5% per cycle) (Table A2). A sequential injection moulding process simulated the mechanical recycling of PMMA, so the PMMA thermal exposure increased over time. The reciprocal degree of polymerization (DP) correlated linearly with the number of cycles (Figure 2) indicating a similar molecular weight loss mechanism between each cycle.[34] We attribute this loss to the volatilization of small compounds from random chain scission during the regrinding and melt-mixing step. From Table A2, we can verify that after 5 cycles of mechanical recycling, the chemical structure of the polymer was slightly degraded.

3.2 | Tensile and impact test

The variation in yield strength and strength at break of PMMA were minor and fell in the range of uncertainty

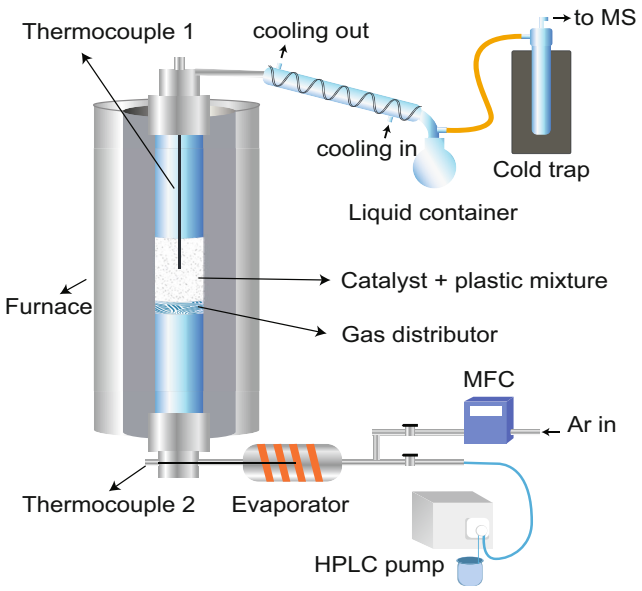

FIGURE 1 Micro-fluidized bed reactor for poly (methyl methacrylate) (PMMA) recycling scheme.

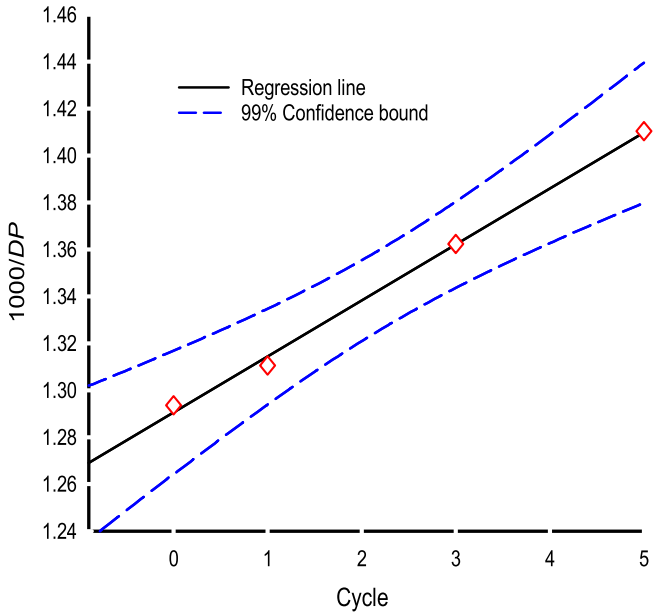

FIGURE 2 Correlation between the reciprocal of *DP* with the recycling cycle.

for experiment data. Young's modulus followed a similar trend as deviation in each cycle was less than 10% despite the decrement of average molecular weight. As the polymer heats up over the mechanical recycling cycles, the intra- molecular void expands, which dislocates the polymer molecules and reduces the PMMA's impact strength. The polymer impact strength decrease correlates with the intra-molecular free volume over the

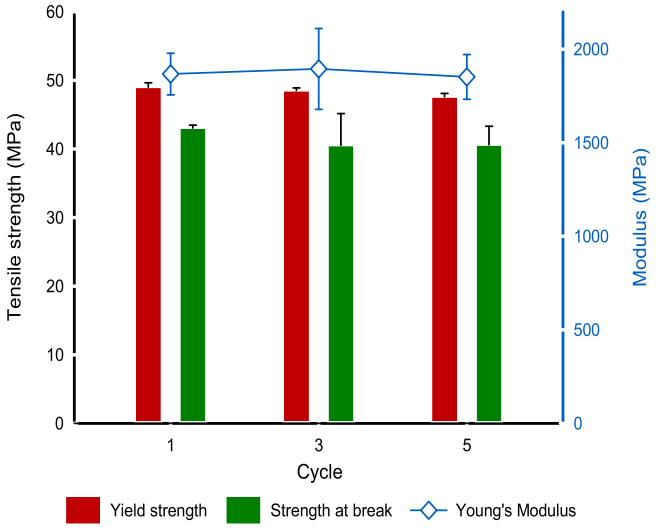

FIGURE 3 Variation of tensile properties with recycling cycle.

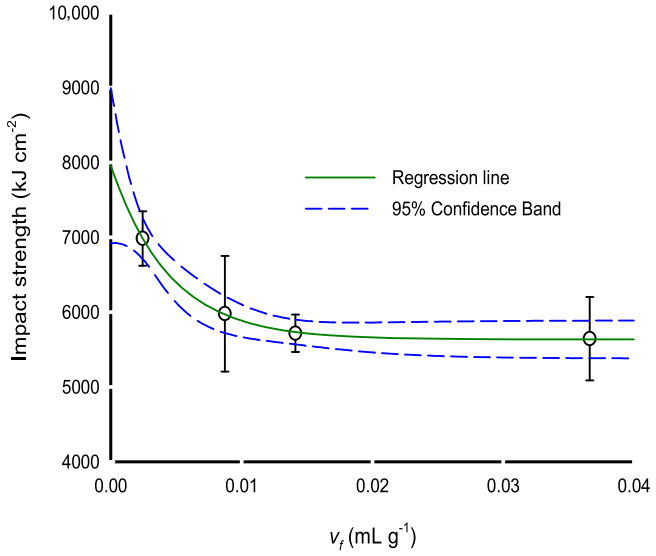

FIGURE 4 Variation of impact strength and free volume with recycling cycle.

5 cycles (Figures 3 and 4). Another reason for the loss of impact resistance comes from the polymer matrix's energy absorption capacity loss due to random chain scission.[6] This result also indicated that bulk elasticity and tensile resistance of PMMA are not sensitive to thermal treatment after 5 cycles of mechanical recycling, which is in good agreement with the literature.[35,36]

3.3 | Optical properties analysis

From visual inspection, there was a visible change in colour with the number of cycles. The samples from the first cycle were transparent, and yellowness kept increasing

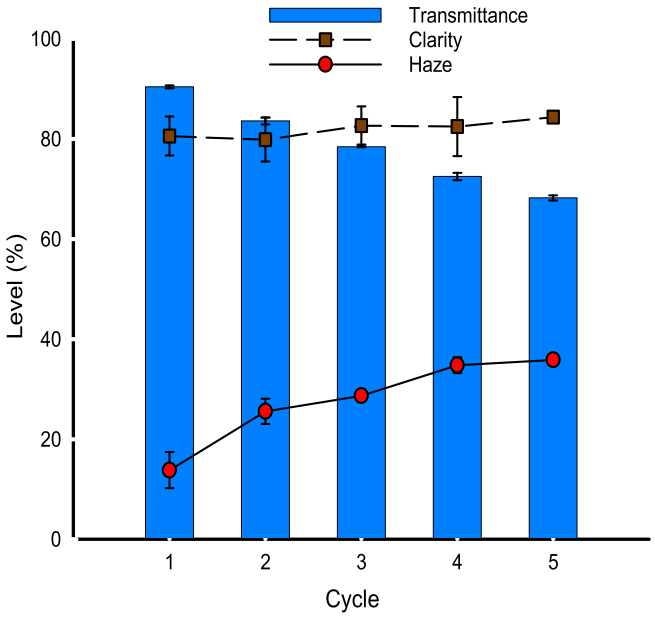

FIGURE 5 Variation of impact strength and free volume with recycling cycle.

until the cycle 5, with the final colour being greyish brown and fully opaque. As compression moulding samples representing cycle 0 do not have a good surface, only injection moulding (cycle 1–5) samples are representative of the optical test. Among 3 properties, clarity has the least variation with a slight increase from 80% to 84.4%. The free volume expansion after each cycle gave PMMA chains more space for movement, causing intra-molecular rearrangement and refractive index shift.[6] This causes the total transmittance to drop sharply from 90.4% to 68.2% throughout 5 cycles (Figure 5). During the injection moulding process, a small fraction of polymer degrades with the volatilization of short carbon chains, which creates impurities in the material structure.[37] These impurities shift the absorbance band of polymers to visible light. For this reason, the plastic specimens turn yellow and the transmittance decreases.[38] Additionally, the haze level increases with the number of recycling cycles starting from 14% (Figure 5). This abnormally high haze level at cycle 1 is due to the substantial distortion of the sample surface in the injection moulding process.[39]

3.4 | Catalyst characterization

The XRD patterns of γ-Al_2O_3 displays 3 peaks at $2\theta = 67.1^\circ$, 45.6°, and 37.2°, which corresponded to reflections from (4 4 0), (4 0 0), and (3 1 1) planes, respectively (Figure A1). The peaks were relatively broad due to the high content of amorphous structure. The commercial FCC diffracts giving sharp peaks that represent

TABLE 3 Catalysts' physical characteristics.

Characteristics	γ-Al_2O_3	FCC	Sand	SiC
U_{mf} (mms^{-1})	4.5	3.8	11.3	14.3
S_{tot} (m^2g^{-1})	140	260.0	45	0
V_{pore} (mLg^{-1})	0.3	0.1	0.0	0.0
d_{pore} (nm)	4.9	3.8	1.9	1.9
ρ_{bulk} (gmL^{-1})	0.91	0.78	1.33	1.50
d_{10} (μm)	79	64	58	81
d_{50} (μm)	96	85	73	128
d_{90} (μm)	121	114	88	191

Abbreviations: FCC, fluid-cracking catalyst; SiC, silicon carbide.

the faujasite crystalline phase of zeolite Y (Figure A1).[40] Kaolinite crystalline scattered X-ray at characteristic $2\theta = 24.8^\circ$, 20.4°, and 12.4° which correspond to (0 0 2), (−1 1 0), and (0 0 1) planes.[41] A small fraction of quartz (SiO_2) was detected, showing the high scattering effect on planar surface (0 1 1), $2\theta = 26.7^\circ$, confirming the composition of commercial FCC.[41]

γ-Al_2O_3 specific surface area is 136.4 m^2g^{-1} and pore diameter of 4.9 nm which lies in the mesoporous material range (2 nm $\leq d_{pore} \leq$ 50 nm) (Table 3). The FCC has higher specific area of 261 m^2g^{-1} comparing to Al_2O_3. Both catalysts have particle sizes in the range of 63 − 106 μm after being sieved (Table 3). The high surface area of both catalysts along with active catalytic sites was expected to improve the yield of MMA in PMMA depolymerization. Sand and silicon carbide are heavier than catalysts (ρ_{bulk} = 1.33 and 1.50 g mL^{-1}, respectively). SiC and sand are both Geldart type B particles, but sand particles are finer and more dispersed while SiC particles are bigger and prone to agglomeration (Table 3).[24,42] Sand is also more porous than SiC with a total surface area of 45 m^2g^{-1} (Table 3).

3.5 | Effect of cracking catalysts on PMMA pyrolysis

PMMA and catalyst particles were fluidized together in an inert environment of Ar to maximize the plastic–catalyst contact. The bed was heated at 80°C/min to reach the target temperature after 4–5 min. During the ramp, melted PMMA became sticky and sintered the surrounding particles, causing bed defluidization. However, we noticed that a fast ramp to 380°C shortened the defluidization time to 30 s–1 min, while at 350°C the bed required 15 min to refluidized again. Another key factor in maintaining stable fluidization is high gas velocity (around 10 U_{mf}) that kept the solid moving and reduced the adhesive

force between particles. Nevertheless, a high fluidization gas velocity and fast temperature ramp raise the number of hot spots inside the reactor which caused coking reactions and reduction of catalytic activity of the bed.[43]

Pyrolysis products were separated into 3 types: solid, liquid, and gas phases. The main component in the liquid phase is methyl methacrylate (MMA). Methanol, ethyl methacrylate, butanol, and n-butyl methacrylate were detected in the mixture at trace levels (Figure A7). The yield of acetone is calculated in Table 5. Notably, isobutene was also detected, albeit at concentrations below the limit of quantification (LOQ). In general, a large amount of product remained in the solid phase while the liquid recovery was as low as 2% for the FCC bed (Figure 6). The percentage of organic compound in solid phase while using FCC remained consistently between 60% and 70%, while for γ-Al_2O_3, this number varied depending on reaction conditions. The recovered liquid fraction was significantly higher over alumina bed with a peak of 46% for run 5. Meanwhile, FCC converted PMMA into more gaseous products with the maximum gas phase composition by mass of 16% for run 9.

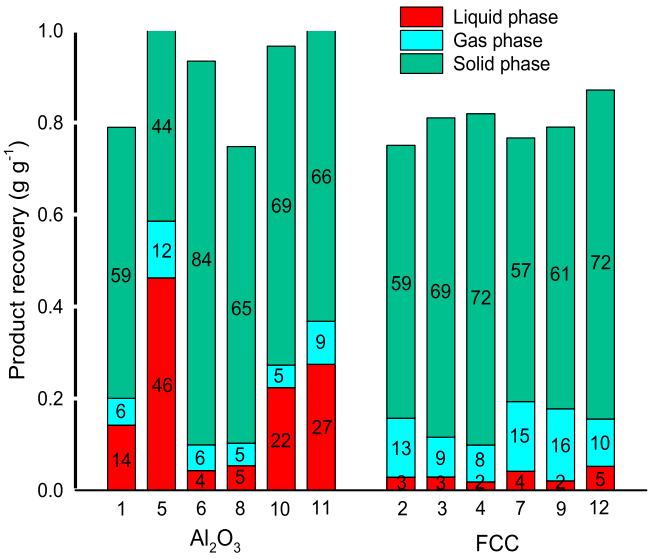

FIGURE 6 Total carbon recovered from poly (methyl methacrylate) (PMMA) pyrolysis over γ-Al_2O_3 and fluid-cracking catalyst (FCC) beds (Table 4).

Catalyst type is one of the critical factors affecting the monomer yield from PMMA pyrolysis. While the highest PMMA conversion over γ-Al_2O_3 bed was 65% at 380°C, FCC activated PMMA degradation with conversion ranging from 64% to 95% (Table 4). However, FCC showed no selective catalytic activity since both yield and selectivity toward MMA were less than 4% in every experiment. Most of the products stayed in the solid phase in form of char (Figure 6) due to the high cracking ability of FCC. The strong reactivity of FCC bed also directed the pyrolysis toward valorization of plastic to the uncondensable vapour which contributes to 13%–25% of carbon mass lost during experiment (Figure 6). As the carbon content in the gas phase is harder to quantify than solid and liquid phases, non-condensable gases at low concentrations were not able to quantify. Furthermore, PMMA depolymerization follows a random scission mechanism, leading to the formation of MMA oligomers.[15] These compounds in the liquid phase are challenging to quantify

TABLE 4 Design of experiment with affiliated result.

Catalyst (run)	T (°C)	U_g (mm s^{-1})	m (g)	X_{PMMA}[a] (%)	Y_{MMA} (%)	S_{MMA} (%)
Al_2O_3 (1)	380	38	10	43	14	33
FCC (2)	380	38	10	95	2	2
FCC (3)	350	38	7	64	2	2
FCC (4)	350	50	7	75	1	2
Al_2O_3 (5)	380	50	7	65	46	71
Al_2O_3 (6)	350	50	10	23	4	17
FCC (7)	380	38	7	88	3	3
Al_2O_3 (8)	350	38	10	33	5	15
FCC (9)	380	50	10	85	1	2
Al_2O_3 (10)	350	38	7	22	20	90
Al_2O_3 (11)	350	50	7	43	27	62
FCC (12)	350	50	10	74	1	2

Abbreviations: FCC, fluid-cracking catalyst; MMA, methyl methacrylate; PMMA, poly (methyl methacrylate); TGA, thermogravimetric analysis.

[a]Determined by TGA.

TABLE 5 Byproducts composition from decomposition of 1 g poly (methyl methacrylate) (PMMA).

Run order	Yield (%)			
	CO	CH_4	CO_2	Acetone
1	1	3	2	0
2	7	1	5	1
3	6	1	2	1
4	3	1	4	1
5	0	1	11	0
6	2	2	1	0
7	8	1	6	1
8	2	2	2	1
9	5	1	10	1
10	2	1	1	3
11	2	1	7	1
12	7	1	3	4

using the GC–MS method, resulting in a loss of carbon recovery.

Meanwhile, temperature has the most impact on MMA yield with run 5 had the highest Y_{MMA} of 46% at 380°C and 7 g of Al_2O_3. At 30°C lower, the yield reduced to 27%. The conversion rose proportionally with temperature when keeping similar fluidizing velocity and catalyst weight. Increasing the amount of Al_2O_3 to 10 g diluted the overall PMMA concentration and decreased the tendency to defluidize. Additionally, γ-alumina load expansion increases the probability of side reactions and worsens the MMA selectivity; it reached a peak of a mass fraction of 90% at run 10 (Table 4). However, the bed defluidized in approximately 15 min during the experiment as gas velocity was only 38 mms^{-1} which is insufficient to break the particle agglomeration. Therefore, PMMA conversion in this run reached the lowest level of 22%.

MMA degrades through head-tail side-group β scission mechanism giving $CH_3O(CO)\cdot$ radical.[18] The further decomposition of $CH_3O(CO)\cdot$ produces CO_2 and $CH_3\cdot$ which transforms into CH_4 by absorbing hydrogen.[18] Hence, if it was only for MMA decomposition, the amount of CO_2 and CH_4 would be expected to be equivalent. However, the concentration of CO_2 was higher than CH_4, suggesting that there was another side reaction that can produce CO_2.[44] $CH_3O(CO)\cdot$ also degrades by another mechanism into CO and CH_3OH. At T > 350°C, the $CH_3O(CO)\cdot$ fragment prioritized degrading into CO_2 and CH_4.[45,46] The methanol recovered in the liquid phase was detected at a trace amount, but there was a noticeable amount of CO in the gas phase which suggests

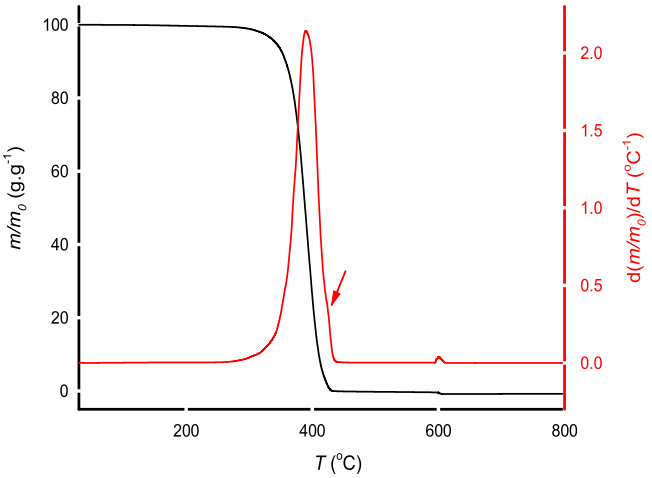

FIGURE 7 Thermal gravimetric analysis (black curve) and derivative thermogravimetry (red curve) of poly (methyl methacrylate) (PMMA) under N_2 and air atmosphere (60 mL/min).

that methanol rapidly decomposes into volatiles. The low flow velocity (38 mms^{-1}) and low temperature (350°C) favoured the formation of acetone (Table 5).

3.6 | Solid samples analysis

PMMA pellets have a M_w of 120,100 g mol^{-1} and T_g of 109°C which suggests an atactic macromolecular structure.[47] From the DTG curve, PMMA started degrading at 260°C and the degradation rate reached a peak at 390°C (Figure 6).[48] A small shoulder from the main peak appeared at 420°C due to the coking reaction of the remaining PMMA, creating carbon-rich compounds (Figure 7).[49,50] These compounds burned when we switched the atmosphere from N_2 to air at 600°C and the sample was completely consumed, closing the global mass balance.

PMMA catalytic pyrolysis solid residue over γ-Al_2O_3 bed degraded in 4 stages under N_2 (Figure A5). The first peak at 220°C corresponds to the moisture adsorbed by the solid residue. The next two sharp weight loss peaks from 220 to 420°C and above 420°C are associated with the decomposition of PMMA to volatile compounds and coke, respectively. The last peak at 600°C correlates with the coke burn after switching the atmosphere from N_2 to air. The data set was in good agreement with the TGA profile from pure PMMA (Figure 7). At 350°C and bed weight of 10 g, the increase of fluidization velocity from 38 to 50 mm s^{-1} slightly degraded more plastic (runs 6 and 8, Figure 8). However with 7 g of γ-Al_2O_3 and at 350°C, reducing the flow velocity resulted in 20% lower PMMA conversion between run 10 and 11 (Figure 7). The reason is the defluidization of run 10 due to the

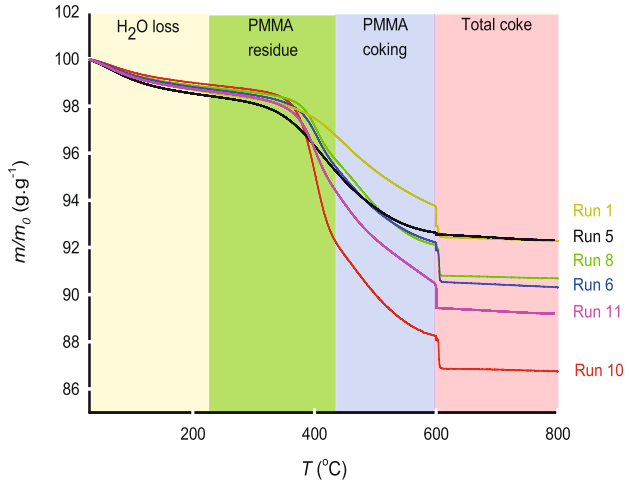

FIGURE 8 Thermal gravimetric analysis of solid residue from poly (methyl methacrylate) (PMMA) pyrolysis with γ-Al_2O_3 bed under N_2 and air atmosphere (60 mL/min).

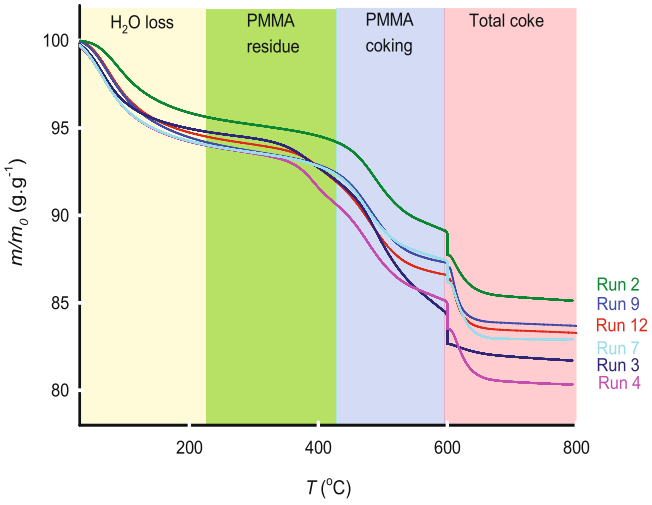

FIGURE 9 Thermal gravimetric analysis of solid residue from poly (methyl methacrylate) (PMMA) pyrolysis with fluid-cracking catalyst (FCC) bed under N_2 and air atmosphere (60 mL/min).

lower velocity which decreases the local mixing rate. Meanwhile, at 380°C run 1 (10 g Al_2O_3) has lower plastic conversion compared to run 5 (7 g Al_2O_3) but obtained a higher coke content. Therefore, the TGA results further confirm the decisive role of Al_2O_3 load and fluidization velocity on PMMA conversion. Following a similar trend, at 380°C, velocity 50 mm s^{-1}, run 2 (10 g FCC) has 10% more coke than run 7 (7 g FCC) (Figures 8 and 9). The solid residues from reacted FCC beds contained up to 35% coke as opposed to γ-Al_2O_3 solid residues that were coke-free. Besides that, with 10 g FCC, run 9 (380°C) has similar coke content compared to run 12 (350°C). This investigation verified the high cracking ability of FCC that converted PMMA into unwanted char precursors

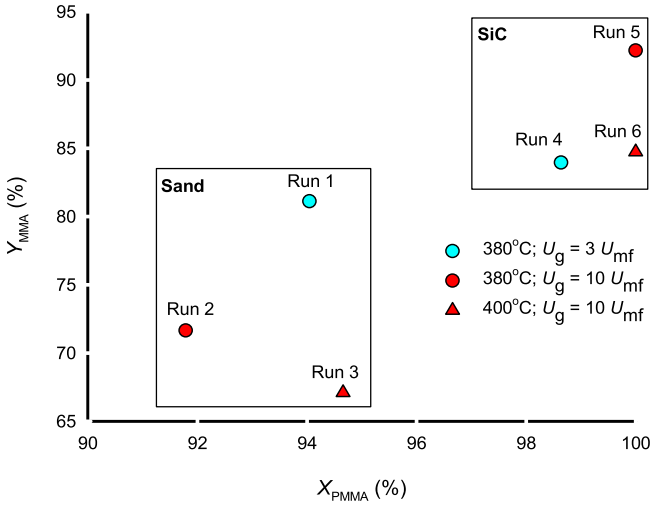

FIGURE 10 Effect of reaction condition on methyl methacrylate (MMA) yield over sand and silicon carbide (SiC) bed.

even at 350°C. This temperature is lower than conventional operating temperature of a fluidized bed reactor for PMMA pyrolysis.[7,15,20]

3.7 | Non-catalytic PMMA pyrolysis over SiC and sand bed

The reactor contained inert heat transfer media and PMMA was rapidly heated to 380 or 400°C.[21,51–53] The bed started becoming segregated at 130°C and defluidized in 2 min for sand until the temperature reached 350°C. With SiC media, the bed at $U_g = 3\ U_{mf}$ was completely defluidized above $T = 150$°C, while at high gas velocity (10 U_{mf}), it started fluidizing again after reaching 380°C. In both cases, the molten plastic bonded particles to create agglomerated chunks. These chunks grew heavier and segregated at the bottom of the bed, which progressed to total bed defluidization.[54] However, sand particles are smaller and less dense than SiC particles (Table 3), and chunks are lighter and break apart at lower gas velocities (3 U_{mf}). SiC bed yielded more MMA (ranging from 84% to 92%) compared to sand (67%–85%) (Figure 10). This comes from the higher density of SiC compared to sand, resulting in higher specific heat capacity (Cp) and better heat transfer of SiC bed.[25] MMA yielded maximum at 380°C, $U_g/U_{mf} = 10$ on SiC bed. At 400°C PMMA converted fully in the SiC bed, but the MMA yield lowered by 7% compared to the test at 380°C due to the formation of by-products CO_2, CH_4, and acetone (Tables 6 and 7). The percentage ratio of CH_4–CO_2 was equal which means they were generated from $COOCH_3\cdot$ decomposition (Table 6).[46] Meanwhile, CO/methanol ratios in experiments at 380°C were roughly 2:1, while at 400°C

TABLE 6 Gas composition from pyrolysis of poly (methyl methacrylate) (PMMA) over 7 g of silicon carbide (SiC)/sand bed.

Run order	Yield (%) CO	CH_4	CO_2
1	4	1	1
2	6	1	2
3	2	10	9
4	1	4	4
5	3	0	0
6	2	4	5

TABLE 7 Liquid and solid composition from pyrolysis of poly (methyl methacrylate) (PMMA) over 7 g of silicon carbide (SiC)/sand bed.

Run order	Yield (%) Acetone	Methanol	Coke
1	0	2	4
2	5	2	5
3	0	2	5
4	0	2	4
5	0	2	3
6	0	2	3

these values were only 1:1 suggesting a transformation of methanol at lower temperature to form trace amount of dimethyl ether (DME).[20] Acetone was detected in sand bed (run 2) at 5%, while it was not in SiC (Table 7). We attributed this phenomenon to the higher specific surface area of sand than SiC (Table 3), which trapped air to form acetone.[55]

3.8 | PMMA pyrolysis mechanism over FCC and γ alumina bed

To investigate the degradation mechanism of MMA over FCC and alumina, we injected the pure MMA into hot catalytic beds. From the DOE results, high temperature (380°C) and low velocity (38 mm s^{-1}) is preferred for higher conversion of MMA (Table 8). Liquid phase analysis recorded a significant difference between MMA recovery of 93% from alumina bed in comparison with 36% from FCC bed. While only 2% of organic compound remained in Al_2O_3 bed, FCC over-cracked MMA in solid–gas fluidized bed to 29% of carbon-rich coke. Therefore, FCC not only unzipped the PMMA chains to form MMAs but also further cracked these monomers into other volatile compounds and coke. γ-Al_2O_3, on the other hand, has less effect on MMA degradation (Table 8).

TABLE 8 Composition of main products from MMA pyrolysis at 380°C, $U_g = 38$ mm s^{-1} over 10 g of FCC/γ-Al_2O_3.

Catalyst	Conversion (%)	MMA (%)	Solid residue (%)
FCC	64	36	29
γ-Al_2O_3	7	93	2

Abbreviations: FCC, fluid-cracking catalyst; MMA, methyl methacrylate.

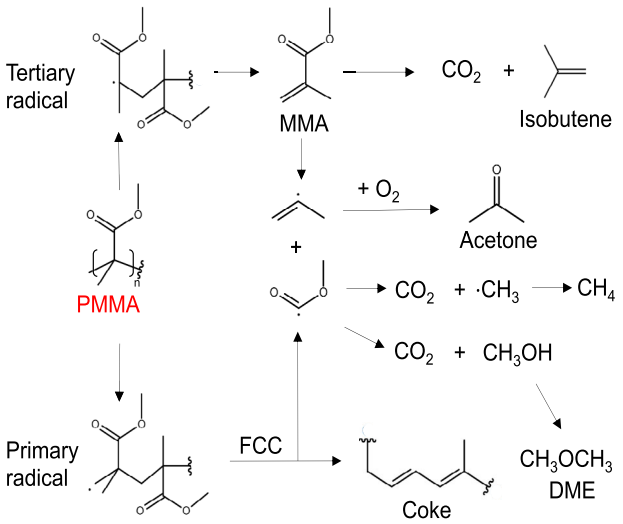

FIGURE 11 Mechanism of poly (methyl methacrylate) (PMMA) depolymerization in fluidized bed. Fluid-cracking catalyst (FCC) cracked methyl methacrylate (MMA) into CO, CO_2, CH_4 and char which was verified by experiment. Acetone was also derived from a part of this reaction.

Here we proposed the mechanism for PMMA degradation over FCC and Al_2O_3 (Figure 11). The main peak from DTG curve at around 400°C indicates a random scission of polymer chains (Figure 7),[56,57] creating tertiary and primary alkyl radicals. Random thermal scission progresses through the unzipping of end groups from tertiary radicals to release MMA. FCC activated the primary radicals to undergo side group β fission to smaller fragments as methyl formate radicals and rich carbon compounds with conjugated carbon chains, while Al_2O_3 did not.[44,49,58] Further degradation of $COOCH_3\cdot$ produced CO_2 and CH_4. The sudden rise in CO_2 concentration could stem from the degradation of MMA to CO_2 and uncondensable isobutene (Figure A7).[45,46] Additionally, β C-C bonds in MMA dissociated by FCC into $COOCH_3\cdot$ and allyl radicals which combine with oxygen absorbed by catalysts to form acetone. Methyl formate radicals degraded in another pathway forming CH_3OH and CO at a molar ratio of 1:1. However, the lack of CH_3OH in the recovered liquid phase suggested that 2 molecules of CH_3OH lost 1 water molecule to form

dimethyl ether (DME) which is evacuated through ventilation.[15,59,60]

4 | CONCLUSIONS

Partial thermal degradation is the main issue associated with mechanical recycling for impact-modified PMMA. After 5 cycles of grinding and re-injection moulding, the tensile strength, break strength, and tensile modulus variated marginally. However, impact strength reduction follows a non-linear regression model when the free volume rises. This was explained by the relaxation of polymer chain in expanded intramolecular void. As this free volume rises along with number of recycling cycles, the impact strength will decrease drastically that material will become more brittle. The optical properties were also susceptible to thermal treatment with decrement in transmittance and increment in haze level up to 22%. Free volume elevation and thermal degradation were attributed to these changes. Hence, PMMA mechanical recycling is appropriate for polymer-to-polymer strategy but in different applications that do not require high optical or impact resistance properties such as decoration or household appliances.

PMMA pyrolysis provides an effective way to retrieve valuable compounds from waste plastic. In this study, we pyrolyzed impact-modified PMMA in a fluidized bed with γ-Al_2O_3 and FCC catalysts. At temperatures lower than 400°C, alumina bed exhibited low catalytic activity since the maximum yield of MMA recovered was only 46%, while FCC has no selectivity toward monomer but forming up to 35% of coke. The pyrolysis experiments with pure MMA confirmed the highly reactive effect of FCC that over-cracked this monomer through a viable transition step into char and other by-products. The DOE result from catalytic beds identified that catalyst types, weight, and temperature are critical to MMA recovery. Contrary to mixed plastic or polyolefin, PMMA depolymerizes better in non-catalytic beds.[61] The novel SiC bed achieved the highest yield of 92% at 380°C, which is comparable to literature results using sand as fluidizing media at 20–70°C and more.[7,20,51] The inert and non-porous characteristics of SiC are key factors to prevent PMMA from over-cracking and side reactions.

AUTHOR CONTRIBUTIONS

Tien Dat Nguyen: Visualization; writing – original draft; formal analysis; data curation; conceptualization; methodology; investigation; validation. **Nooshin Saadatkhah:** Writing – review and editing; investigation. **Yanfa Zhuang:** Investigation; writing – review and editing. **Jacopo De Tommaso:** Writing – review and editing; investigation. **Karen Stoeffler:** Project administration; resources; writing – review and editing; funding acquisition; supervision. **Adrien Faye:** Writing – review and editing; resources; investigation. **Gregory S. Patience:** Supervision; writing – review and editing; validation; resources; funding acquisition; project administration; conceptualization.

ACKNOWLEDGEMENTS

The authors thank the National Research Council of Canada (NRC) Collaborative Science, Technology and Innovation Program (CSTIP) (AM-102-1) for the resources and financial support of the project 'Recycling Technologies for polymer Automotive Components'.

CONFLICT OF INTEREST STATEMENT

The authors declare no potential conflicts of interest.

PEER REVIEW

The peer review history for this article is available at https://www.webofscience.com/api/gateway/wos/peer-review/10.1002/cjce.70004.

DATA AVAILABILITY STATEMENT

The data that support the findings of this study are available from the corresponding author upon reasonable request.

ORCID

Tien Dat Nguyen https://orcid.org/0000-0002-3374-6090

Gregory S. Patience https://orcid.org/0000-0001-6593-7986

REFERENCES

[1] V. M. Research, Polymethyl Methacrylate (PMMA) Market Size & Share to Surpass $7.36 Billion by 2030. **2023** https://www.globenewswire.com/en/news-release/2023/6/5/2681775/0/en/Polymethyl-Methacrylate-PMMA-Market-Size-Share-to-Surpass-7-36-Billion-by-2030-Vantage-Market-Research.html (accessed: June 2024).

[2] J. De Tommaso, J.-L. Dubois, *Polymer* **2021**, *13*, 2724.

[3] S. van der Heijden, *Virtual* **2020**, *15*, 11.

[4] A. R. Prado, A. G. Leal-Junior, C. Marques, S. Leite, G. L. de Sena, L. C. Machado, A. Frizera, M. R. N. Ribeiro, M. J. Pontes, *Opt. Express* **2017**, *25*, 30051.

[5] C. Capone, L. Di Landro, F. Inzoli, M. Penco, L. Sartore, *Polym. Eng. Sci.* **2007**, *47*, 1813.

[6] Z. Q. Liu, A. M. Cunha, X.-S. Yi, A. C. Bernardo, *J. Appl. Polym. Sci.* **2000**, *77*, 1393.

[7] W. Kaminsky, C. Eger, *J. Anal. Appl. Pyrolysis* **2001**, *58–59*, 781.

[8] E. Esmizadeh, S. Khalili, G. Vahidifar, A. Naderi, C. Dubois, *Waste Polymethyl Methacrylate (PMMA): Recycling and High-Yield Monomer Recovery*, Springer International Publishing, Cham, Switzerland **2018**, p. 1.

[9] Y. Zhuang, N. Saadatkhah, M. S. Morgani, T. Xu, C. Martin, G. S. Patience, A. Ajji, *Can. J. Chem. Eng.* **2023**, *101*, 59.
[10] D. L. Dunkelberger, (Rohm and Haas Company) *US4440905*, 1985.
[11] A. Walther, K. Matussek, A. H. E. Müller, *ACS Nano* **2008**, *2*, 1167.
[12] M. Röttger, T. Domenech, R. van derWeegen, A. Breuillac, R. Nicolaÿ, L. Leibler, *Science* **2017**, *356*, 62.
[13] A. López, I. de Marco, B. Caballero, A. Adrados, M. Laresgoiti, *Waste Manag.* **2011**, *31*, 1852.
[14] Z. Chen, X. Zhang, F. Yang, H. Peng, X. Zhang, S. Zhu, L. Che, *Appl. Catal. A Gen.* **2021**, *609*, 117.
[15] O. V. Chub, N. Saadatkhah, J.-L. Dubois, G. S. Patience, *Appl. Catal. A: Gen.* **2022**, *638*, 118.
[16] S. Khangkham, Catalytic degradation of poly(methyl methacrylate) by zeolites and regeneration of used zeolites via ozonation. **2012** https://oatao.univ-toulouse.fr/9227/ (accessed: May 2024).
[17] S. Sakkosit, S. Damronglerd, C. Ngamcharussrivichai, *Adv. Mater. Res.* **2013**, *622*, 1173.
[18] E. K. Moens, K. De Smit, Y. W. Marien, A. D. Trigilio, P. H. Van Steenberge, K. M. Van Geem, J.-L. Dubois, D. R. D'hooge, *Polymer* **2020**, *12*, 1667.
[19] B. Singh, N. Sharma, *Polym. Degrad. Stab.* **2008**, *93*, 561.
[20] W. Kaminsky, J. Franck, *J. Anal. Appl. Pyrolysis* **1991**, *19*, 311.
[21] G. Lopez, M. Artetxe, M. Amutio, G. Elordi, R. Aguado, M. Olazar, J. Bilbao, *Chem. Eng. Process. Process. Intensif.* **2010**, *49*, 1089.
[22] U. Arena, M. L. Mastellone, *Chem. Eng. Sci.* **2000**, *55*, 2849.
[23] J. Moseley, T. O'Brien, *Chem. Eng. Sci.* **1993**, *48*, 3043.
[24] D. Geldart, *Powder Technol.* **1973**, *7*, 285.
[25] M. Díaz-Heras, A. Calderón, M. Navarro, J. A.-I. nez, A. I. Fernández, C. Barreneche, *Sol. Energy Mater. Sol. Cells* **2021**, *219*, 110.
[26] ASTM, *D638 Standard Test Method for Tensile Properties of Plastics*, ASTM International, West Conshohocken, PA **2014**.
[27] ASTM, *256 Standard Test Methods for Determining the Izod Pendulum Impact Resistance of Plastics*, ASTM International, West Conshohocken, PA **2018**.
[28] D. Walsh, P. Zolle, *Standard Pressure Volume Temperature Data for Polymers*, Technomic, Lancaster, PA **1995**.
[29] Y. Zhuang, N. Saadatkhah, T.-D. Nguyen, J. De Tommaso, C. Y. J. Ng, C. Wang, A. Ajji, G. S. Patience, *React. Chem. Eng.* **2025**, *10*, 237.
[30] H. Li, J. Li, J. Bodycomb, G. S. Patience, *Can. J. Chem. Eng.* **2019**, *97*, 1974.
[31] K. Smolders, *Waste Manage.* **2004**, *24*, 849.
[32] D. Kunii, O. Levenspiel, *Fluidization and Mapping of Regimes*, Butterworth—Heinemann, Stoneham, MA **1991**, p. 71.
[33] M. Menéndez, J. Herguido, A. Bérard, G. S. Patience, *Can. J. Chem. Eng.* **2019**, *97*, 2383.
[34] A. Emsley, R. Heywood, *Polym. Degrad. Stab.* **1995**, *49*, 145.
[35] H. Zhang, S. Sellaiyan, K. Sako, A. Uedono, Y. Taniguchi, K. Hayashi, *Polymer* **2020**, *190*, 122.
[36] Y. Zhao, R. Huang, Z. Wu, H. Zhang, Z. Zhou, L. Li, Y. Dong, M. Luo, B. Ye, H. Zhang, *Mater. Des.* **2021**, *202*, 109.
[37] X. Colin, J. Verdu, *C. R. Chim.* **2006**, *9*, 1380.
[38] S. S. Suresh, S. Mohanty, S. K. Nayak, *Journal of Remanufacturing* **2017**, *7*, 217.
[39] V. Kalima, J. Pietarinen, S. Siitonen, J. Immonen, M. Suvanto, M. Kuittinen, K. Monkkonen, T. Pakkanen, *Opt. Mater.* **2007**, *30*, 285.
[40] M. Treacy, J. Higgins, *Collection of Simulated XRD Powder Patterns for Zeolites*, 5th ed., Elsevier Science B.V, Amsterdam, Netherlands **2007**, p. 174.
[41] J. Anthony, R. Bideaux, K. Bladh, M. Nichols, *Mineral. Mag.* **2001**, *65*, 152.
[42] Y. Cui, W. Fu, Y. Zhang, X. Cao, P. Xu, M. A. Rehan, B. Li, *Chem. Eng. Process.* **2020**, *154*, 108016.
[43] M. Artetxe, G. Lopez, M. Amutio, G. Elordi, M. Olazar, J. Bilbao, *Ind. Eng. Chem. Res.* **2010**, *49*, 2064.
[44] S. I. Stoliarov, P. R. Westmoreland, M. R. Nyden, G. P. Forney, *Polymer* **2003**, *44*, 883.
[45] R. L. Forman, H. M. Mackinnon, P. D. Ritchie, *J. Chem. Soc. C.* **1968**, 2013.
[46] W. R. Zeng, S. F. Li, W. K. Chow, *J. Fire Sci.* **2002**, *20*, 401.
[47] L. Chang, E. M. Woo, *Polym. Chem.* **2010**, *1*, 198.
[48] N. Saadatkhah, A. Carillo Garcia, S. Ackermann, P. Leclerc, M. Latifi, S. Samih, G. S. Patience, J. Chaouki, *Can. J. Chem. Eng.* **2020**, *98*, 34.
[49] B. Holland, J. Hay, *Polymer* **2001**, *42*, 4825.
[50] M. Ferriol, A. Gentilhomme, M. Cochez, N. Oget, J. Mieloszynski, *Polym. Degrad. Stab.* **2003**, *79*, 271.
[51] A. Sasaki, T. Tsuji, in *The 5th Sympos. Feedstock Mechan. Recycl. Polym. Mater. (ISFR2009)*, Chengdu, China **2009**, pp. 79–83.
[52] G. Grause, M. Predel, W. Kaminsky, *J. Anal. Appl. Pyrolysis* **2006**, *75*, 236.
[53] R. S. Braido, L. E. P. Borges, J. C. Pinto, *J. Anal. Appl. Pyrolysis* **2018**, *132*, 47.
[54] M. Balland, K. Froment, G. Ratel, S. Valin, J. Roussely, R. Michel, J. Poirier, Y. Kara, A. Galnares, *Waste Biomass Valoriz.* **2017**, *8*, 2823.
[55] T. A. Homan, Fine sand in motion: the influence of interstitial air. **2013** https://research.utwente.nl/en/publications/fine-sandin-motion-the-influence-of-interstitial-air (accessed: January 2024).
[56] T. Fateh, F. Richard, T. Rogaume, P. Joseph, *J. Anal. Appl. Pyrolysis* **2016**, *120*, 423.
[57] C. B. Godiya, S. Gabrielli, S. Materazzi, M. S. Pianesi, N. Stefanini, E. Marcantoni, *J. Environ. Manage.* **2019**, *231*, 1012.
[58] T. Kashiwagi, A. Inabi, A. Hamins, *Polym. Degrad. Stab.* **1989**, *26*, 161.
[59] A. L. Moghaddam, M. J. Hazlett, *J. Environ. Chem. Eng.* **2023**, *11*, 110.
[60] A. Bakhtyari, M. Parhoudeh, M. R. Rahimpour, *J. Nat. Gas Sci. Eng.* **2016**, *28*, 31.
[61] Y.-H. Lin, M.-H. Yang, *Appl. Catal. A: Gen.* **2007**, *328*, 132.

SUPPORTING INFORMATION

Additional supporting information can be found online in the Supporting Information section at the end of this article.

How to cite this article: T. D. Nguyen, N. Saadatkhah, Y. Zhuang, J. De Tommaso, K. Stoeffler, A. Faye, G. S. Patience, *Can. J. Chem. Eng.* **2026**, *104*(1), 31. https://doi.org/10.1002/cjce.70004